BBAA VI International Colloquium on:
Bluff Bodies Aerodynamics & Applications
Milano, Italy, July, 20–24 2008

SENSITIVITY OF THE WAVE-STEEPENING IN RAILWAY TUNNELS WITH RESPECT TO THE FRICTION MODEL

Stefan Adami[⋆] and Hans-Jakob Kaltenbach[¶]

[⋆]work carried out when affiliated with DB Systemtechnik
now with: Lehrstuhl für Aerodynamik, Technische Universität München
Boltzmannstraße 15, 85748 Garching, Germany
e-mail: *stefan.adami@aer.mw.tum.de*

[¶]Deutsche Bahn AG, DB Systemtechnik, Aerodynamics and Air conditioning
Völckerstraße 5, 80939 München, Germany
e-mail: *hans-jakob.kaltenbach@bahn.de*

Keywords: Tunnel aerodynamics, micro-pressure wave, sonic boom, wave-steepening, unsteady friction model

Abstract: *A one-dimensional model for the numerical prediction of the propagation of a compression wave through a slab-track equipped railway tunnel is validated using field data collected in 2006 in two nearly* $8\,km$ *long tunnels on the new German high-speed line connecting Nuremberg and Ingolstadt. The sensitivity and ambiguity of the prediction with respect to the choice of the friction model is demonstrated. The wave attenuation of acoustical absorbers is well prescribed by an increase of the weight of the unsteady friction term. Comparison of the wave steepening prior and after installation of acoustical absorbers shows that the efficiency of the absorbers depends on the characteristic frequency of the wave.*

It is shown that the design of an optimal entry wave shape - for example by modification of the geometry of the train nose or the tunnel entry section - depends somewhat on the choice of friction parameters. If the unsteady friction term exceeds a certain value an entry wave with a short rise time is more attenuated than a comparable wave which reaches its maximum gradient at a later instance of the wave passage. However, with respect to contributions to the sound spectrum in the audible range an entry wave with a nearly symmetrical shape performs better than either waves with short or long rise times.

1 INTRODUCTION

In the late 1970s the emission of the so-called micro-pressure waves (MPW) from tunnel portals became an issue on the Japanese Shinkansen high-speed network when train speed increased above $200\,km/h$ [18]. When the train enters the tunnel it acts like a semi-permeable piston. A compression wave forms ahead of the train which propagates through the tunnel at the speed of sound. The non-linear, gas-dynamic processes cause a steepening of the wave up to the possibility to form a shock if the tunnel is sufficiently long - in the order of $10\,km$ - and if frictional losses are small. When the wave is reflected at the opposite portal an impulsive wave is emitted into the surroundings which consist primarily of infrasound. The amplitude of this pressure pulse - the MPW - is approximately proportional to the maximum pressure gradient of the compression wave approaching the tunnel exit.

By now it is well understood what factors determine the intensity of the MPW and the associated possible nuisance and environmental impact. The magnitude of the pressure gradient created during train entry depends on train speed - approximately to the third power - , on the blockage, i.e. the ratio of cross-sectional area of train to tunnel, on the shape and the length of the train head, and on the geometry of the tunnel entrance.

The process of wave steepening during propagation along the tunnel is governed by the tunnel length, by the frictional losses, and by the presence of side branches and changes in cross sections in the tunnel. Large differences of the growth rate of the maximum pressure gradient have been observed for ballasted track and for slab track. When the tunnel exceeds a certain length further wave steepening is inhibited.

As a consequence, emission of micro-pressure waves is most critical for tunnels with small cross sections that are equipped with slab track, which have a length in the order of 5 to $10\,km$, and where the operational speed exceeds $250\,km/h$.

So far, MPW emission has not been a pressing issue on European networks for several reasons: most tunnels on existing high-speed lines are double track and have larger cross sections than in Japan where $A_{tun} = 64\,m^2$ on Shanyo Shinkansen. Also, some tunnels with a critical length or small cross sections are equipped with ballasted track. In addition, on most lines operational speeds are not as high as in Japan.

For example, on the German line segments between Cologne and Frankfurt and between Ingolstadt and Nuremberg where maximum speeds up to $300\,km/h$ are reached the cross section is $92\,m^2$. Tunnels on the lines Hannover-Würzburg and Stuttgart-Mannheim have smaller cross sections of $A_{tun} \approx 82\,m^2$ but operational speed does not exceed $250\,km/h$. In addition, the two longest tunnels Landrücken ($10.8\,km$) and Mühlberg ($10.2\,km$) are (partially) equipped with ballasted track. Nevertheless, audible MPWs had been observed on the northern portal of the Mühlberg tunnel during test runs with the ICE-V when operated at speeds up to $380\,km/h$.

In France, the $4.8\,km$ long, single track Villejust tunnel near Paris is rather narrow with only $46\,m^2$ cross section for each of its two tubes. However, MPW emission is not an issue there since it is equipped with ballasted track and since operational speed is limited to $220\,km/h$.

Audible MPWs had been produced by purpose at the $2700\,m$ long Terranuova Le Ville tunnel (cross sectional area $A_{tun} = 67\,m^2$) on the line Rome-Florence within the research project TRANSAERO [13] and at the $4500\,m$ long Schulwald tunnel on the line Cologne-Frankfurt/Main [7, 8] by letting two trains simultaneously enter the tunnel on parallel tracks from the same direction, thereby reaching a blockage of $R = A_{train}/A_{tun} \approx 0.21$.

With the new line Nuremberg-Ingolstadt going in operation in the summer of 2006 the propagation of compression waves created during the tunnel entry of high speed trains has received

renewed interest within Deutsche Bahn since two tunnels on the line reach a length in the order of $8\,km$. Initially, a ballasted trackbed was planned. Later, this was changed into slab track. As a result, the decrease of wave attenuation due to the change in the trackbed surface led to the emergence of noticeable MPW emissions when the line was tested prior to opening. In order to alleviate this problem both tunnels were equipped with sound absorbing material [2, 20] which allowed the line to go into operation without delay and without restrictions.

Within Deutsche Bahn AG the need for accurate prediction methods for the wave steepening has increased since new lines currently under planning or construction will be equipped with slab track and will have single-track tunnels with cross sections of $60\,m^2$ [6]. In addition, the topic had received some attention within the context of maglev transportation [11, 21].

The main challenge for a one-dimensional numerical analysis of the wave propagation consists in the modeling of the friction effects. Side branches, air shafts, niches, and cross-sectional changes can be treated with satisfactory accuracy within the framework of acoustic theory [16, 15, 4, 5].

The sound-absorbing properties of a ballast bed have been modeled in terms of an acoustic model - a series of Helmholtz resonators - for a porous surface [16, 15, 23], and in terms of an equivalent circuit analysis [17]. More recently, it was concluded that the effect could equivally well be captured by the so-called unsteady friction term [3].

The unsteady friction term was introduced by Zielke [29] in the context of friction modeling in the one-dimensional approximation of hydraulic networks. For laminar flow the term can be derived analytically since it arises solely from the reduction of the problem dimensions across the stream tube. Physically, when a uniform velocity disturbance propagates along a tube the friction effects are felt immediately at the walls. They diffuse from the tunnel walls into the core flow, causing a time delay between different layers of the stream tube. As a consequence the flow history - the past accelerations - appears in a one-dimensional approach where the flow is considered as uniform across the stream tube.

The concept of unsteady friction was extended to turbulent flows along smooth and rough walls in [28, 25, 27]. One of the first applications of an unsteady friction model in tunnel aerodynamics is reported in [19].

The prediction of wave propagation in tunnels is routinely carried out at the RTRI by the use of one-dimensional codes with the friction model parameters adjusted to give good agreement with measurements in tunnels with slab track or ballasted track [3, 5]. Other implementations of 1-D-codes and their validation against experimental data are reported in [24, 1].

The purpose of this paper is to document the background and the state-of-art of a one-dimensional simulation tool developed at DB Systemtechnik for the prediction of the wave propagation. The emphasis is on verification - through comparison with an analytical solution - and validation by comparison with field data collected on the Euerwang tunnel of the Nuremberg-Ingolstadt line. As a side topic the potential of wave shape optimization within the context of the development of countermeasures is studied which has recently received some attention [14].

The paper is organized in the following way: in section 2 some details on the implementation of the friction model are given and the verification of the model is described. Results are presented in section 3, including calibration of the friction parameters against measurement data and an investigation of the wave shape influence on MPW emission when an unsteady friction model is used.

2 METHOD

2.1 Computational approach

As in [5] the one-dimensional Euler equations augmented by the two source terms $4\,\tau_W/d_h$ and $4\,\tau_{us}/d_h$ modeling "quasi-steady" and "unsteady" friction according to

$$\frac{\partial\left(\rho u\right)}{\partial t}+\frac{\partial\left(\rho u^2+p\right)}{\partial x}=-\frac{\lambda}{d_h}\frac{1}{2}\,\rho\,u^2-\epsilon_{us}\frac{16\,\rho\,\nu}{d_h^2}\int\limits_0^t W\left(t-\tau\right)\frac{\partial u(\tau)}{\partial\tau}\,d\tau \tag{1}$$

are solved using the Godunov approach in the implementation of the CLAWPACK library routines [12]. Here, $d_h=4\,A_{tun}/U_{tun}$ denotes the hydraulic diameter of the tunnel and $W(t-\tau)$ is a weighting function which depends on the Reynolds number and the roughness [22, 27]. Heat transfer to the tunnel walls is not included in the model. At each cell interface a Riemann problem is solved based on Roe's approximate solver. Zero-order extrapolation boundary conditions are specified at both ends of the computational domain.

The problem is formulated with respect to a non-moving coordinate system. However, in order to save resources the computational domain which extends over approximately twice the length of the initial wave front - in the order of $100\,m$ - is shifted in the direction of wave propagation at regular intervals of $10\,m$. Each time the domain is shifted, part of the solution at the rearward end of the wave is lost whereas the conditions of air at rest are specified at the newly added grid points ahead of the wave front. The time step is chosen such that the Courant number does not exceed the value of one in the entire domain.

As in [26] the weighting function in the unsteady friction term is approximated efficiently in terms of a series expansion of decaying exponentials according to

$$\tau_{us}\left(t+\Delta t\right)\approx\sum_{i=1}^{N}\left[\tau_i\left(t\right)e^{-\frac{4n_i\nu}{d_h^2}\Delta t}+\frac{\rho m_i d_h}{n_i}\left(1-e^{-\frac{4n_i\nu}{d_h^2}\Delta t}\right)\frac{\partial u}{\partial t}\Big|_{t+\Delta t}\right]\,. \tag{2}$$

Here, n_i and m_i are the coefficients of the N exponentials of the series approximation of W. For every node at each time step the N summands τ_i from the previous time step are used (and updated) which contain the entire previous history of the acceleration $\partial u/\partial t$.

2.2 Unsteady friction model

Different flow states (laminar/turbulent) and roughness parameters enter the unsteady friction term through the weighting function $W(\psi)$ as function of the dimensionless time $\psi=4\nu\theta/d_h^2$ and the Reynolds number $Re=u\,d_h/\nu$ where $\theta=t-\tau$ is the time running backwards. For example, the model of [25] reads

$$W=\frac{1}{2\sqrt{\pi\psi}}e^{-B\psi}\quad,\quad B=\frac{1}{12.86}Re^{\kappa}\quad,\quad\kappa=\log_{10}\left(\frac{15.29}{Re^{0.0567}}\right)\quad. \tag{3}$$

In Fig. 1 three models are compared, namely Zielkes analytical solution [29] for the laminar case and two versions of Vardy & Brown [22, 25] for a turbulent pipe flow with smooth walls. It is evident that the approximations for $W(\psi)$ only differ for dimensionless times $\psi\geq10^{-5}$. On the other hand the maximum spatial extension of a typical compression wave is in the order of $100\,m$ which corresponds to a time of passage of $0.3\,s$ respectively $\psi=2.5\cdot10^{-7}$ for $d_h=8.5\,m$.

Thus, it is no surprise that in the computational example of a typical wave propagation considered in Fig. 1 (right) the steepening proceeds at the same rate for the three different models.

Similarly, for the relevant time scales the consideration of roughness according to [27] corresponds primarily to a (vertical) shift of the entire curve $W(\psi)$ in Fig. 1. Thus, its effect can equally well be captured by an adjustment of the global weight ϵ_{us} of the entire term rather than by a change in W. Apparently, a similar experience was made at RTRI since in the implementation reported in [14] the unsteady friction model of [25] was simplified such that the differences to other models for W disappeared.

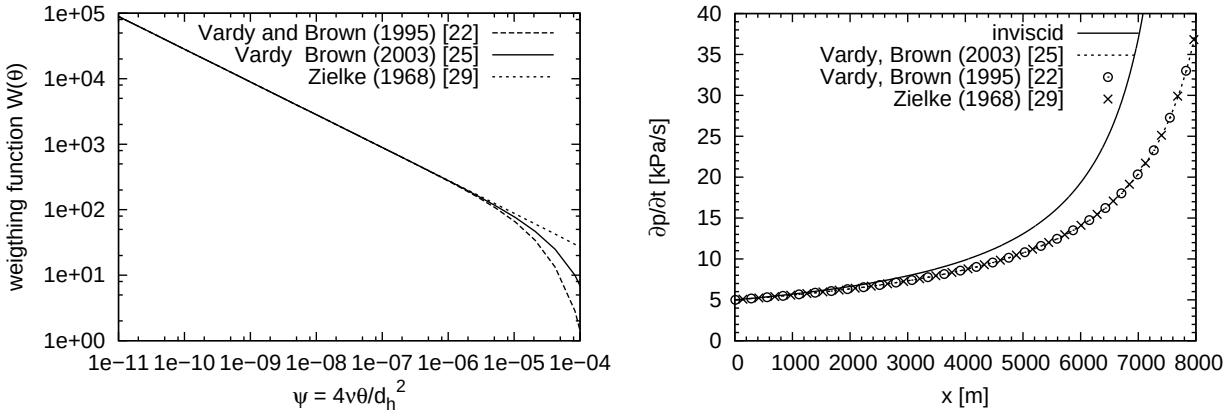

Figure 1: Comparison of three models for the unsteady friction term: Left: different approximations of the weighting function W as function of $\theta = t - \tau$, Right: evolution of the maximum pressure gradient in a simulation with $\lambda = 0$, $\epsilon_{us} = 5$, and three models for W.

2.3 Code verification and check of convergence

The implementation was thoroughly tested and validated by comparison with the analytical solution for the inviscid case. Fig. 2 shows the growth of the maximum pressure gradient for a synthetic polynomial shaped initial wave with $\partial p/\partial x|_{max} = 5000\, Pa/s$ and an amplitude of $1500\, Pa$. The numerical solution starts to deviate from the analytical reference solution after $7500\, m$ propagation. By that time the maximum gradient has increased by an order of magnitude.

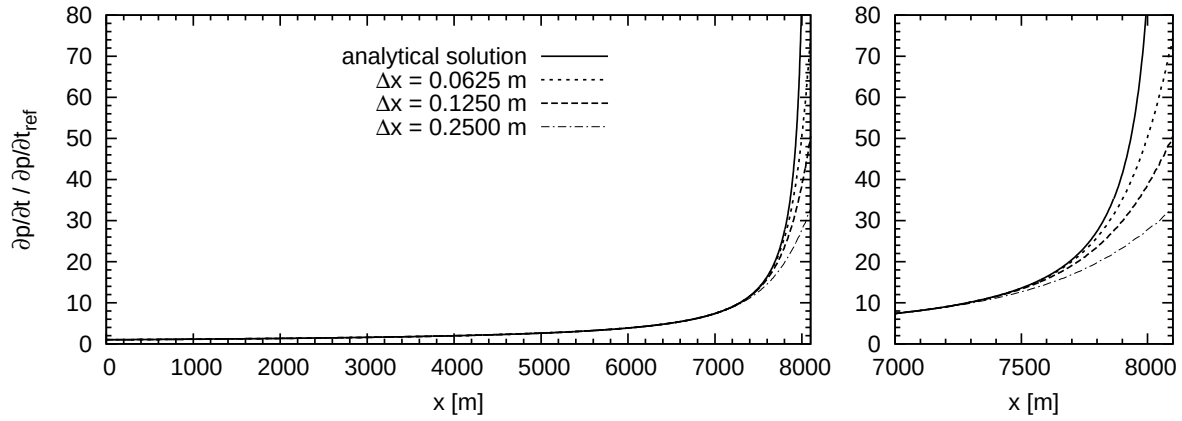

Figure 2: Evolution of the maximum pressure gradient versus propagation distance for mesh sizes of $\Delta x = 0.25\, m$, $0.125\, m$ and $0.0625\, m$.

The implementation based on the Godunov scheme was compared with a McCormack dis-

cretization of second order accuracy in time and space. The superior accuracy of the Godunov scheme compensates for its by a factor of 2.4 higher computational cost per node. This is demonstrated in Fig. 3 which shows that the solution converges faster than for the McCormack scheme.

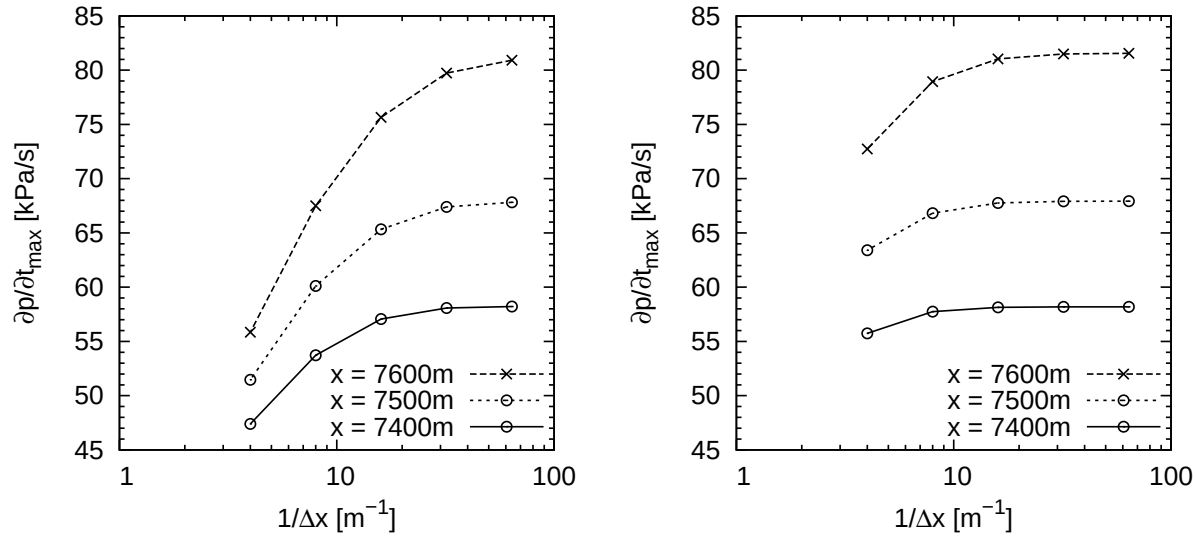

Figure 3: Dependence of the maximum pressure gradient on the spatial resolution $\frac{1}{\Delta x}$ after propagation over $7400\,m$, $7500\,m$, and $7600\,m$ for the McCormack scheme (left) and for the Godunov scheme (right).

When the code is applied for routine investigations the grid independence of the solution is always checked by doubling the resolution. No general rule with respect to the minimum spatial resolution required for obtaining a certain accuracy can be derived solely on the base of the amplitude and the maximum steepness of the initial wave. It has been observed that the curvature in the vicinity of the location where the maximum gradient occurs plays an important role. As a consequence, a resolution criterion based on the third derivative at the inflection point of the entry pressure wave has been derived and proven to be applicable in practice.

3 RESULTS

3.1 Calibration of friction parameters and model validation

In order to use the model for the prediction of the wave propagation in tunnels the friction parameters λ and ϵ_{us} have to be adjusted. This is done subsequently until satisfactory agreement with field data is achieved.

For validation, measurements from two tunnels of the $89\,km$ long double-track line connecting Nuremberg with Ingolstadt are used. From this, a total of $27\,km$ is situated in tunnels with a nominal value of the approximately semi-circular cross section of $92\,m^2$. Most parts of the line are covered with slab track, employing the systems Rheda 2000 (line km 11.5 to 13.6 and 48.6 to 84.6) and Max Bögl (line km 13.6 to 48.6). In the original planning the tunnel interior as well as the entire line was to be built in ballasted track.

Going from north to south the $7700\,m$ long Euerwang tunnel is located between line km 49.145 and 56.854 whereas the $7260\,m$ long Irlahüll tunnel extends from line km 59.564 to 66.824. As shown in Fig. 4 (left) the tunnel walls have a smooth concrete surface which is interrupted in regular intervals by seams. The interior is equipped with installations holding the catenary, signals, lighting, and other items related to safety and emergency handling. In regular

intervals of approximately $1000\,m$ there are small niches with a depth of $2\,m$ that are closed by pressure-tight doors leading to emergency exits, see Fig. 4 (upper right)

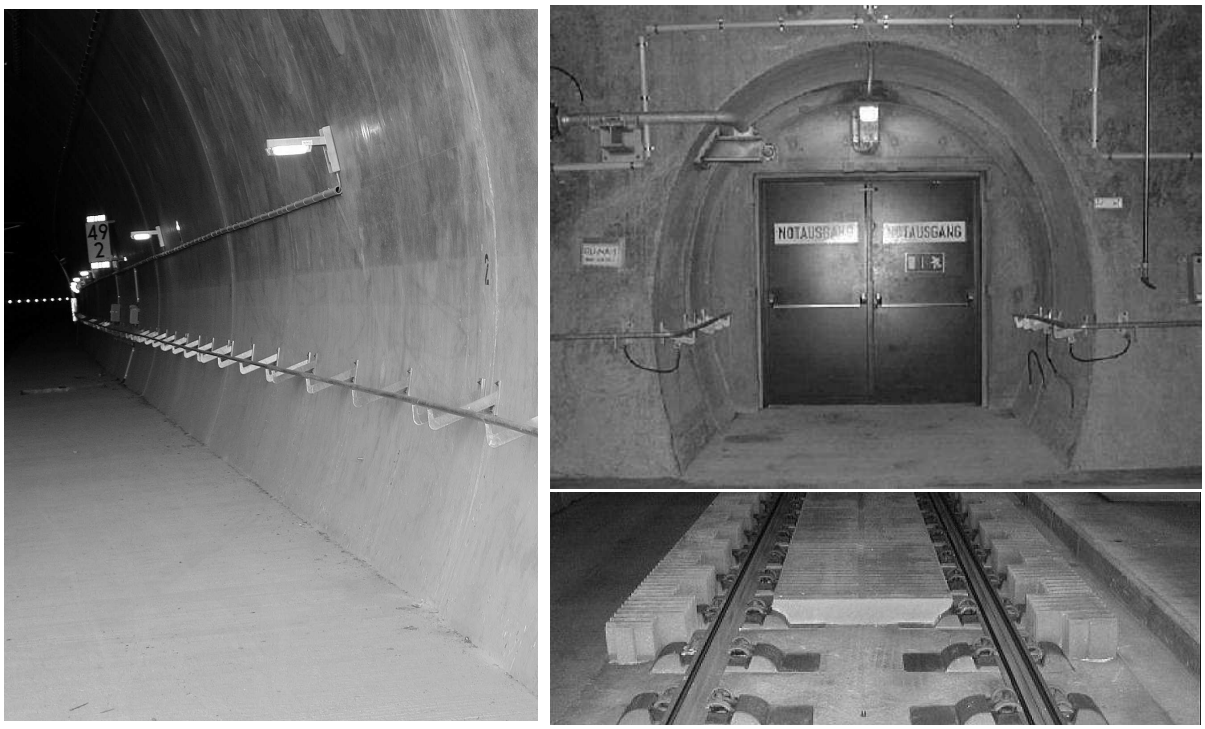

Figure 4: Interior of the Euerwang tunnel.

Fig. 4 also shows the track bed, consisting in a flat concrete surface from which shallow ends of sleepers protrude on which the rails are mounted. Acoustical absorbers were mounted in between the rails and to some extent outside of the track as shown in Fig. 4 (lower right).

In 2006 prior to the line going into operation the wave propagation in the tunnel was measured by installing pressure probes in about $200\,m$ distance from the portals and in between in regular intervals of approximately $1400\,m$. A wide range of entry pressure waves was recorded from the passage of different train heads (ICE 3 and the ICE-S test train with the same nose shape as the ICE 1) cruising at speeds up to $330\,km/h$.

The recorded pressure time series had to be low-pass filtered in order to allow for a reliable determination of the wave steepness, i.e. the pressure gradient, to be compared with model predictions. Two types of low-pass filters were used which yielded similar results. The first method consisted in a cubic spline fit of the curve $p(t)$ for which the parameters were derived using least-squares minimization of the error. The spacing t_{spline} of the nodes of the interpolating splines was adapted to the increasing steepness of the compression wave - characterized by the rise time $t_{wave} = \Delta p/(\partial p/\partial t|_{max})$ - according to $t_{spline}/t_{wave} \approx 0.07...0.12$. The second method consisted in the use of a 4th order Butterworth filter with a cut-off frequency $f_{cut} \approx 80/t_{wave}$.

The measurement of such a rapid pressure rise poses a challenge when the wave develops into a shock. Therefore, some strong MPW events with uncertain accuracy were not included in the validation process. The code validation focuses on the range of pressure gradients which are relevant in practice, namely $\partial p/\partial t|_{max} < 80\,kPa/s$.

As initial conditions for the model predictions the low-pass filtered pressure recordings from a position in about $200\,m$ distance from the tunnel portals were used. From this, the initial values for density and velocity were derived based on the isentropic relations for a simple, right

traveling wave.

Fig. 5 shows an example for wave steepening in the Euerwang tunnel prior to installation of the acoustical absorbers. The friction parameters λ and ϵ_{us} were varied until the best average agreement for an ensemble of about 30 test runs at different speeds was reached. In order to arrive at such a good agreement both parameters λ and ϵ_{us} had to be assigned non-zero values simultaneously. Similar to [3, 5] a value of $\lambda = 0.04$ gave good agreement with respect to reproduction of the slow decay of the wave amplitude. We found that significantly lower values of the unsteady friction parameter had to be used than the values of $9 < \epsilon_{us} < 11$ reported in [3, 5]. This might indicate that there exist some currently unknown differences among slab-track equipped tunnels in Japan and in Germany which have a subtle influence on the wave steepening process.

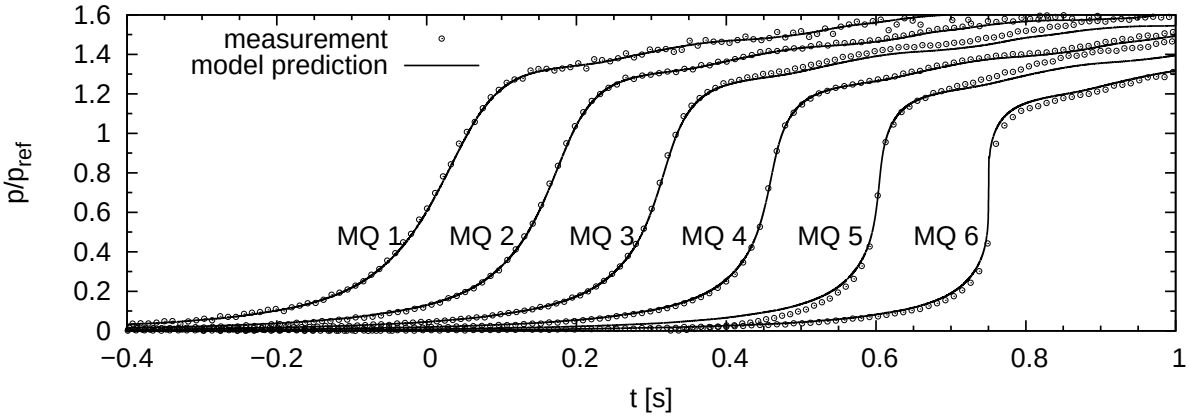

Figure 5: Comparison of measured and simulated wave shape at six locations in the tunnel prior to installation of acoustical absorbers. For clarity, only a subset of the recorded samples is shown.

Fig. 6 (left) shows the wave steepening in condensed form by considering the relative increase of the maximum pressure gradient over segments of $1460\,m$ length. Due to the pre-filtering of the measurements the scatter has been considerably reduced compared to a similar plot shown in [20]. Fig. 6 demonstrates that the wave steepening can be accurately modeled over a considerable range of pressure gradients, covering approximately a 10-fold increase of the steepness of the initial wave.

The ensemble of propagating waves used for the validation includes waves resulting from train passages in both directions of the tunnels. Since portal shapes differ at both tunnel ends the entry pressure wave differs too. This has some consequences for the further assessment and quantitative description of the wave steepening. In the inviscid case the steepening is independent of the wave shape and depends on the maximum initial gradient and the value of the pressure at the location of the maximum initial gradient.

If a friction model is included a detailed numerical analysis based on synthetic entry waves with the same nominal value of $\partial p/\partial t|_{max}(0)$ shows that the steepening rate - expressed in terms of $\partial p/\partial t|_{max}(x)$ - is no longer independent of the wave form. Thus, it is not entirely correct to describe the wave steepening rate in terms of a single curve as done in Fig. 6 and 8. Nevertheless, for the primary range of interest with maximum pressure gradients at the tunnel exit below $20\,kPa/s$ the wave-shape dependence is small and can be neglected given the considerable uncertainties in the measurements and in the determination of the pressure gradient.

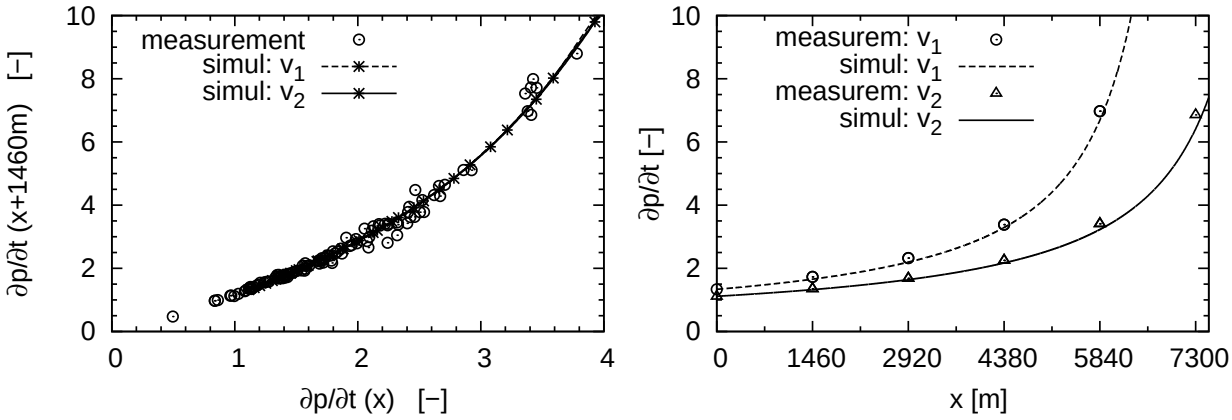

Figure 6: Wave-steepening prior to installation of absorbers: Left: Maximum pressure gradient (in arbitrary units) after propagation through a segment of length 1460 m. Right: evolution of the maximum pressure gradient along the tunnel for two train speeds v_1 and v_2.

Installation of the acoustical absorbers as shown in Fig. 4 (lower right) changed the wave-steepening significantly despite the fact that only 1% of the tunnels cross section was occupied by the porous material. Fig. 7 and 8 show a comparison of model predictions and measurements for this case.

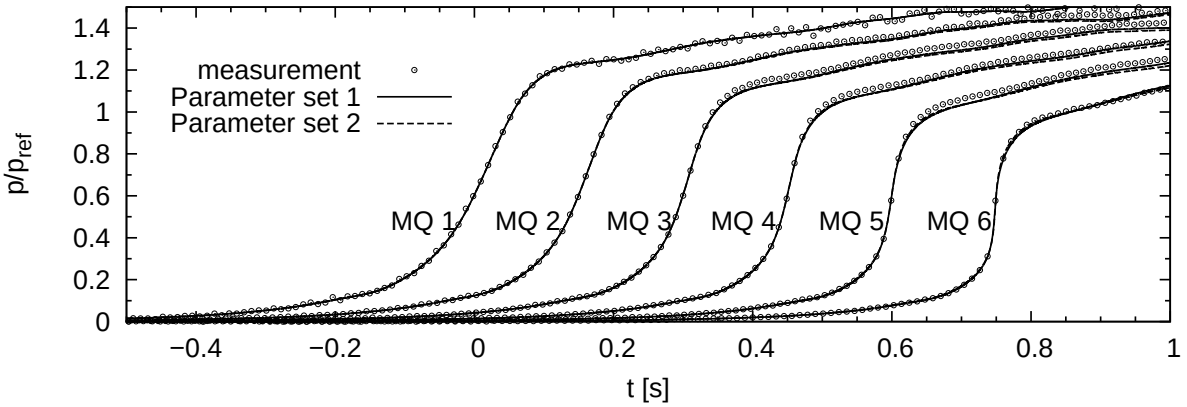

Figure 7: Comparison of measured and simulated compression wave (in arbitrary units) at six locations in the tunnel after installation of acoustical absorbers. Only a subset of the measurements is shown.

These plots demonstrate the very good agreement of the model with respect to the slowly decreasing amplitude and the steepness of the wave which is crucial for the accurate prediction of the emitted infrasound wave at the tunnel exit. Again, both parameters λ and ϵ_{us} had to be assigned non-zero values simultaneously. Nevertheless, it was found that different combinations of λ and ϵ_{us} gave comparable good predictions. This non-uniqueness of the proposed model approach emphasizes the need for a better theoretical foundation. Ideally, a relation between the model friction parameters and some characteristic parameters of the tunnel walls, the trackbed, and other installations such as catenary and signals should be developed. The installation of sound absorbers in the trackbed has a significant impact on the wave steepening which demonstrates the strong sensitivity of this process with respect to small modifications in the surface conditions of tunnel walls and the addition of porous material.

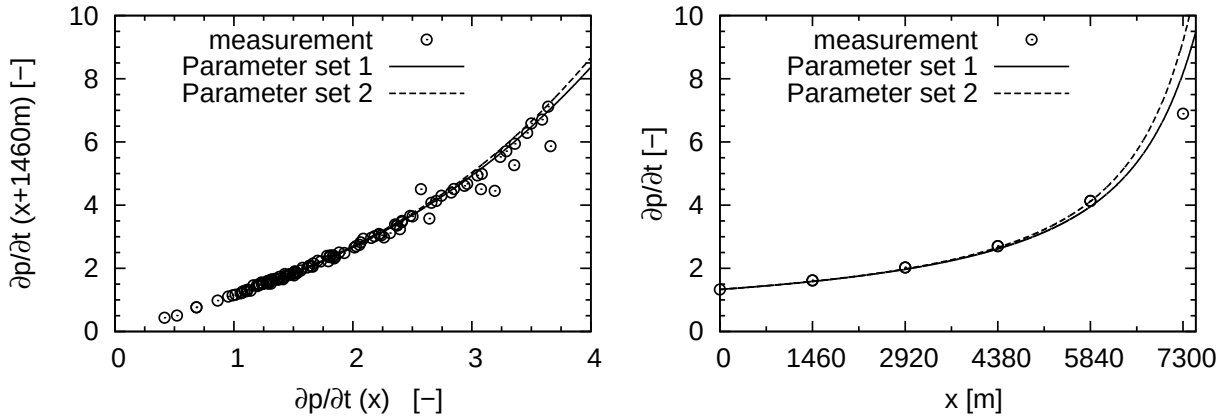

Figure 8: Comparison of wave-steepening after installation of absorbers for two sets of friction parameters. Left: Maximum pressure gradient (in arbitrary units) after propagation through a segment of length 1460 m. Right: evolution of the maximum pressure gradient along the tunnel.

3.2 Effect of absorbers

The wave steepening over segments with a length of $1460\ m$ can be expressed as

$$\xi_{1460m} = \frac{\frac{\partial p}{\partial t}|_{max}(x+1460m)}{\frac{\partial p}{\partial t}|_{max}(x)} \quad . \tag{4}$$

It is plotted against $\partial p/\partial t|_{max}(x)$ in Fig. 6 and 8. These curves can be approximated by the two functions

$$\xi_{\text{no absorbers}}(C) = \frac{1+K_1C}{1+K_2C^2} \quad \text{and} \quad \xi_{\text{with absorbers}}(C) = C^{(K_3C)} \quad , \quad \text{where} \quad C = \left.\frac{\partial p}{\partial t}\right|_{max}(x) \quad . \tag{5}$$

Thus, the efficiency of the acoustical absorbers can be expressed in terms of

$$\eta_{1460\,m} = \frac{\xi_{\text{no absorbers}} - \xi_{\text{with absorbers}}}{\xi_{\text{no absorbers}}} = \frac{\frac{1+K_1C}{1+K_2C^2} - C^{(K_3C)}}{\frac{1+K_1C}{1+K_2C^2}} \, . \tag{6}$$

This expression is plotted in Fig. 9 as function of the maximum pressure gradient. Assuming an amplitude of $\Delta p = 1000\,Pa$ the horizontal axis can be directly converted into a characteristic frequency $f_{wave} = \partial p/\partial t|_{max}/\Delta p$ of the compression wave.

The plot shows that up to a certain wave steepness corresponding to $f_{wave} < 6\,Hz$ the installation of absorbers has little effect on the steepening. This observation might be of some practical relevance for the installation of absorbers in a single-track tunnel which is always operated in the same running direction. There, it might be more economical to only equip the second half of the tunnel oriented towards the exit portal in which the wave has reached a certain steepness rather than to install the absorbers in the entire tunnel.

However, in case of the $7.7\,km$ long Euerwang tunnel a significant improvement of the wave attenuation was observed when the acoustic absorbers covered the full length as compared to only two stretches of $2\,km$ length - corresponding to about 25 % of the total length - near each portal.

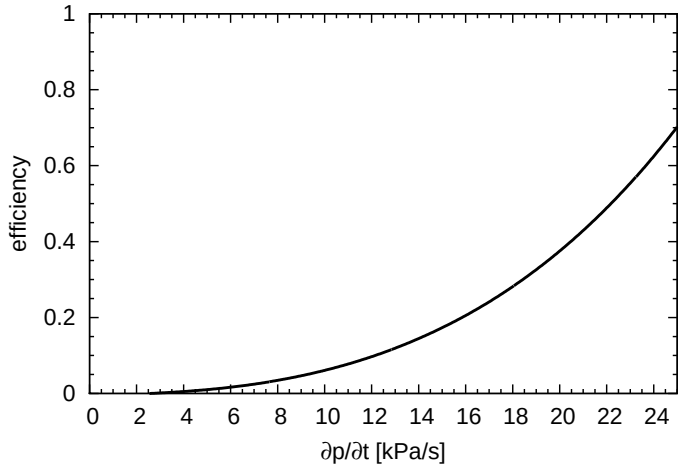

Figure 9: Efficiency of absorbers as function of the maximum pressure gradient of the compression wave. The horizontal axis can also be interpreted as characteristic frequency (in Hz) of the wave.

3.3 WAVE SHAPE OPTIMIZATION

One way to mitigate the steepness of the compression wave consists in the installation of vented hoods or flared portals [18, 9, 10]. By careful design of the cross section and length of the hood and the installation of small side openings in the walls near the portal the shape of the compression wave can be modified.

Ideally, the pressure wave has an almost constant gradient. The primary peak of the emitted pulse is associated with the maximum pressure gradient. In practice, the entry wave from a train entering a hood exhibits several small changes in slope which lead to the emergence of additional peaks. After installation of a tunnel entry hood the size of the openings undergoes some fine tuning in order to optimize the properties of the resulting entry wave with respect to noise emission at the exit portal. The fine tuning allows to adjust the relative size and the order of occurrence of the different peaks of the emitted wave.

Also, in principle it is possible to control the location in the wave front where the maximum pressure gradient occurs. In [14] entry waves were characterized in terms of their 'rise time', i.e. the fraction of time during wave passage it takes to reach the maximum gradient. Thus, a short rise time is typical for a wave which reaches its maximum steepness for a pressure which is well below the half of the disturbance amplitude. Vice versa, a long rise time means that the maximum gradient occurs at a pressure value corresponding to the rear part of the wave front.

Thus, it is interesting to study by numerical simulation how the shape of the entry wave influences the magnitude and frequency content of the emitted wave. This was done in [14] using a one-dimensional model equipped with steady and unsteady friction term as outlined above. In order to reduce the computational effort for an extensive parametric study the numerical tests were carried out using rather high values of the weighting factor ϵ_{us}, thereby exaggerating by purpose the influence of the unsteady friction term on the evolution of the wave.

The use of $\epsilon_{us} \approx 90$ in [14] allowed to stop the simulation after a few hundreds of meters of propagation. Then, some conclusions were drawn by cross comparing results which were all carried out using the same value of ϵ_{us} but different initial wave shapes. Based on these studies it was concluded in [14] that waves with a short rise time are more attenuated during propagation than waves with a long rise time.

In order to study this aspect further we carried out a series of simulations using more realistic values for the friction parameters, namely $\lambda = 0.04$ and $\epsilon_{us} \approx 3$, respectively $\epsilon_{us} \approx 12$. These

values have the same order of magnitude as those used for the prediction of wave propagation on slab track prior and after installation of acoustical absorbers.

Three variants of the initial wave are shown in Fig, 10a. All have the same initial amplitude of $\Delta p = 1500Pa$ and the same maximum gradient $\partial p/\partial t|_{max} = 5kPa/s$ - shown in Fig, 10b - but differ with respect to the location (and accordingly to the pressure) where the maximum gradient occurs, namely at $p = 500\,Pa$, $p = 750\,Pa$, or $p = 1000\,Pa$.

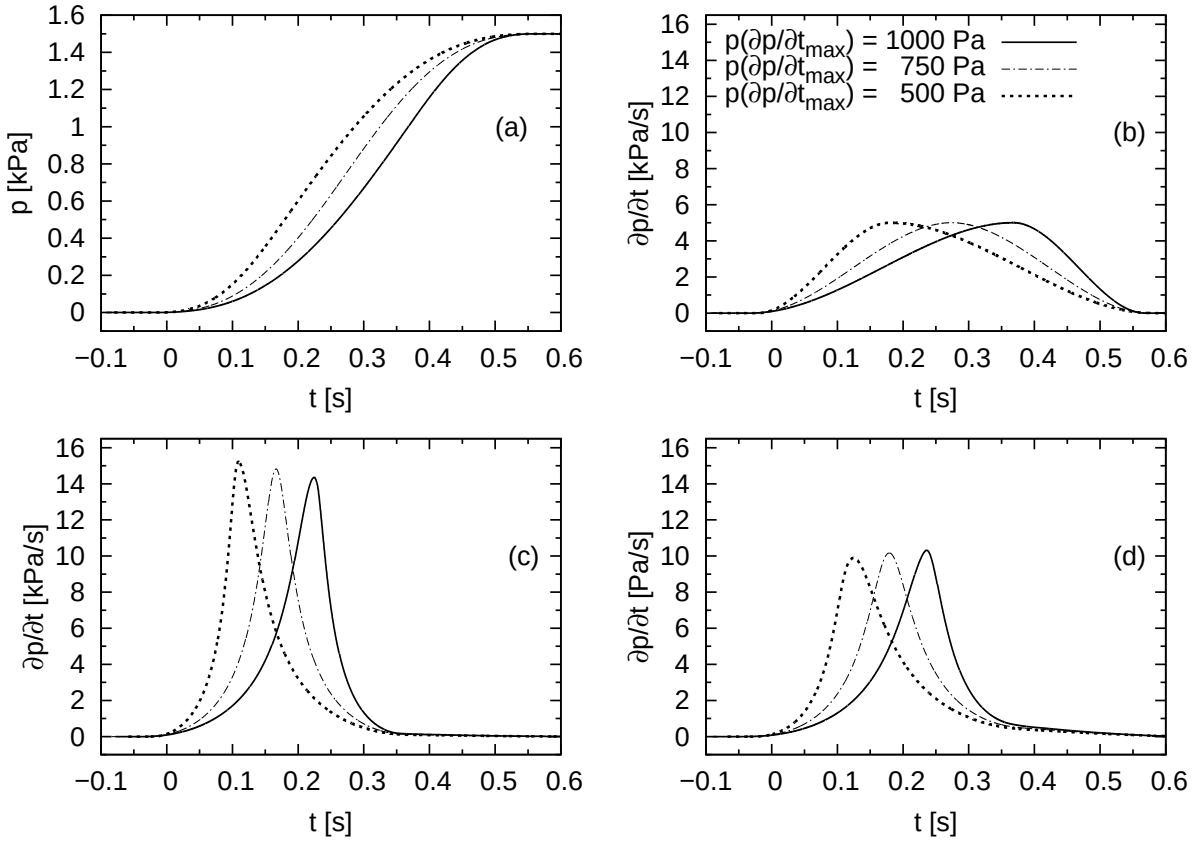

Figure 10: Shape of the initial wave (a),(b) and evolution of the pressure gradient after $6000\,m$ for $\epsilon_{us} \approx 3$ (c) and for $\epsilon_{us} \approx 12$ (d).

Fig. 10 c and d show the resulting waves after $6000\,m$ of propagation. Clearly, the choice of the friction parameter ϵ_{us} has a strong impact with respect to the optimal wave shape. In case of low 'unsteady' friction the wave with the longest rise time steepens at a lower rate than the others. The effect is reversed in case of a higher friction coefficient $\epsilon_{us} \approx 12$. This behavior can clearly be contributed to a change in the relative importance of steady and unsteady friction. Thus, the conclusions on the wave shape influence reported in [14] only apply if the unsteady friction term exceeds a certain value.

The dependency of the wave properties on the friction model is further elucidated by a spectral analysis of the emitted pressure pulse. Based on the exact solution for the sound field emitted by a vibrating piston surrounded by a baffle plate Ozawa et al. [17] derived an estimation formula for the pressure disturbance Δp_{MPW} in the far field as function of the axial distance s from the portal. Using the abbreviations $p' = \partial p/\partial t$, $T_1 = 1.4\,r/c$, $T_2 = r/c$, $k_1 = 1/(4\sqrt{\pi}T_1)$,

and $k_2 = 11/(50\sqrt{\pi}T_2)$ Ozawas model reads

$$\Delta p_{MPW}|_{t+\frac{s}{c}} = \frac{2A_{tun}}{\Omega\, c\,(s+s_0)} \left[\frac{1}{2}p'(t) \quad + \quad k_1 \int_0^t \exp\left(\frac{-\tau^2}{4\,T_1^2}\right) p'(t-\tau)\, d\,\tau \right. \\ \left. + \quad k_2 \int_0^t \frac{\tau}{T_2} \exp\left(\frac{-\tau^2}{4\,T_2^2}\right) p'(t-\tau)\, d\,\tau \right] \quad . \tag{7}$$

Here, $r = 0.5\, d_h$ denotes the (hydraulic) tunnel radius, c denotes the speed of sound, and Ω is the solid angle which depends on the geometry of the portal and its surroundings.

Fig. 11 shows the spectrum of the predicted MPWs in a distance $s = 50\, m$ for the case with $\epsilon_{us} \approx 3$ using $c = 338\, m/s$, $\Omega = \pi$, $A_{tun} = 92\, m^2$, and $d_h = 9.92\, m$.

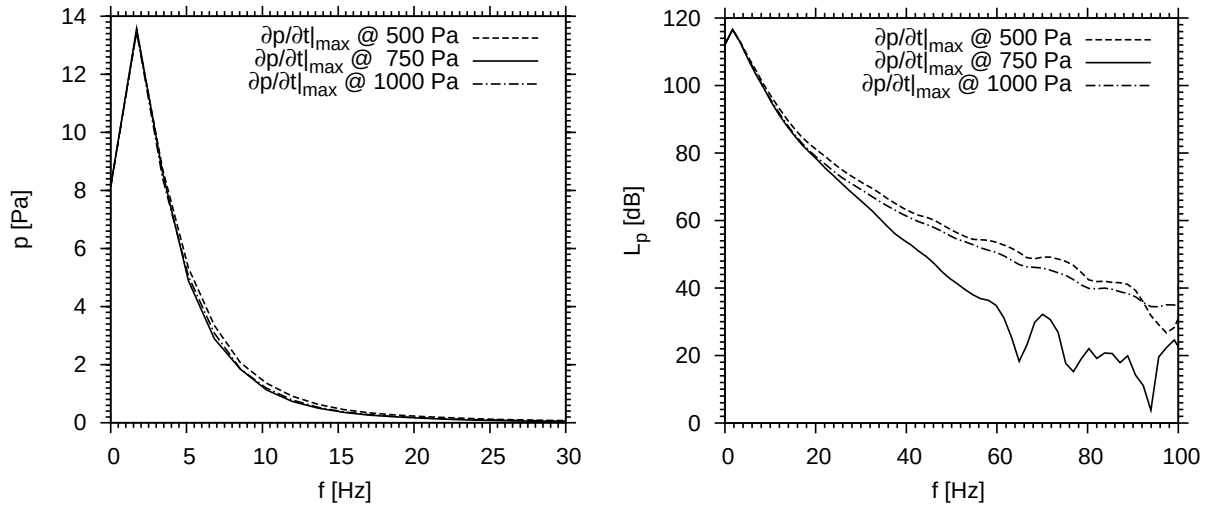

Figure 11: Power spectrum (periodogram) of the emitted pressure pulse after wave propagation for $6000\, m$ using $\epsilon_{us} \approx 3$. The signal was sampled with $3500\, Hz$ over $0.5753\, s$.

It becomes obvious that the MPW signals consist primarily of infrasound with the strongest contributions below $5\, Hz$. Fig. 11 (right) shows that the change in rise time can have a significant effect on the higher frequencies that contribute to the audible part of the signal. With respect to a C-weighting ($L_{C,peak}$) the three waves differ by 0.5 to $1\, dB$. Based on the spectral analysis one can conclude that a wave with a rise time corresponding to half of the time of passage - in other words: a wave which reaches its maximum steepness at half of the amplitude and which has a nearly symmetrical shape - will contribute less in the audible range than either waves with short or long rise time. This shows that the maximum amplitude of the emitted pressure pulse might not be a sufficient criterion for the assessment of its potential harm to the environment.

4 CONCLUSIONS

The compression wave steepening in the long tunnels on the new German high-speed line can be well predicted using state-of-the-art models for the friction effects. For the selection of appropriate model parameters field measurements are needed. The development of the wave shape depends on the friction parameters and the relative weight of quasi-stationary and unsteady friction. The wave attenuation of acoustical absorbers is well prescribed by an increase of the weight of the unsteady friction term. Comparison of the wave steepening prior and after

installation of acoustical absorbers shows that the efficiency of the absorbers depends on the characteristic frequency of the wave.

If the unsteady friction term exceeds a certain value the findings of [14] are corroborated, namely that an entry wave with a short rise time is more attenuated than a comparable wave which reaches its maximum gradient at a later instance of the wave passage. However, with respect to contributions to the sound frequency spectrum in the audible range an entry wave with a medium rise time and nearly symmetrical shape performs better than either waves with short or long rise times.

Wave shape optimization would benefit from a more thorough justification of the friction model.

ACKNOWLEDGMENT

We thank the aerodynamic test team of DB Systemtechnik for providing the measurements collected in 2006 on the line Nuremberg-Ingolstadt.

REFERENCES

[1] A. Baron, P. Molteni, and L. Vigevano. High-speed trains: prediction of micro-pressure wave radiation from tunnel portals. *Journal of Sound and Vibration*, 296:59–72, 2006.

[2] K.-G. Degen, J. Onnich, and C. Gerbig. Acoustic assessment of micro-pressure waves radiating from tunnel exits of DB high-speed lines. *Notes on Numerical Fluid Mechanics and Mulitdisciplinary Design. Bd. 99: Noise and Vibration Mitigation for Rail Transportation Systems, Proceedings of the 9th International Workshop on Railway Noise, Munich, 4 - 8 September 2007. Schulte-Werning, B. et al. (ed.).* Springer. 2008.

[3] T. Fukuda, T. Miyachi, and M. Iida. Propagation of compression wave in a long slab-tracked tunnel and ballast-tracked tunnel. In *Aerodynamics and Ventilation of Vehicle Tunnels, BHR Group, UK*, pages 777–788, 2006.

[4] T. Fukuda, S. Ozawa, M. Iida, T. Takasaki, and Y. Wakabayashi. Propagation of compression wave in a long tunnel with slab tracks. *Quarterly reports of RTRI*, 46(3):188–193, 2005.

[5] T. Fukuda, S. Ozawa, M. Iida, T. Takasaki, and Y. Wakabayashi. Distortion of compression wave propagating through very long tunnel with slab tracks. *JSME International Journal*, 49(4):1156–1164, 2006.

[6] H.-P. Hecht and F. Schaser. Ausbau- und Neubaustrecke Karlsruhe-Basel: Streckenabschnitt 9/Katzenbergtunnel. *Eisenbahntechnische Rundschau*, 55(1/2):39–46, 2006.

[7] J. Herb, P. Deeg, and T. Tielkes. Estimation of the sonic boom effect in future German single-track slab-track tunnels. In *Proceedings of the World Congress on Railway Research, Paper P085*, pages 187–195, 2003.

[8] J. Herb, T. Tielkes, and P. Deeg. Assessment of possible sonic boom effects in German high-speed railway tunnels - experimental and numerical data for the wave-steepening process. In *W. Bradbury (ed.): Proceedings of the 11th International Symposion on Aerodynamics and Ventilation of Vehicle Tunnels '03, Luzern, Switzerland*, pages 775–782. BHR Group Limited, UK, 2003.

[9] M.S. Howe, M. Iida, T. Fukuda, and T. Maeda. Theoretical and experimental investigation of the compression wave generated by a train entering a tunnel with a flared portal. *Journal of Fluid Mechanics*, 425:111–132, 2000.

[10] M.S. Howe, M. Iida, T. Maeda, and Y. Sakuma. Rapid calculation of the compression wave generated by a train entering a tunnel with a vented hood. *Journal of Sound and Vibration*, 297:267–292, 2006.

[11] J. Keil. Projektstand der Magnetschnellbahn München Hauptbahnhof - Flughafen. *Elektrische Bahnen*, 104(10):476–479, 2006.

[12] R.J. LeVeque. *Finite Volume Methods for Hyperbolic Problems*. Cambridge University Press, 2002.

[13] G. Matschke and C. Heine. Full scale tests on pressure wave effects in tunnels. *Notes on Numerical Fluid Mechanics*, 79:187–195, 2002.

[14] T. Miyachi, T. Fukuda, M. Iida, T. Maeda, and S. Ozawa. Distortion of compression wave propagating through Shinkansen tunnel. *Notes on Numerical Fluid Mechanics and Mulitdisciplinary Design. Vol. 99: Noise and Vibration Mitigation for Rail Transportation Systems, Proceedings of the 9th International Workshop on Railway Noise, Munich, 4 - 8 September 2007. Schulte-Werning, B. et al. (ed.).* Springer. 2008.

[15] S. Ozawa, T. Maeda, T. Matsumura, K. Nakatani, and K. Uchida. Distortion of compression wave during propagation along Shinkansen tunnel. In *Aerodynamics and Ventilation of Vehicle Tunnels*, pages 211–215, 1994.

[16] S. Ozawa, T. Maeda, T. Matsumura, and K. Uchida. Effect of ballast on pressure wave propagation through tunnels. In *International Conference on Speedup Technology for Railway and Maglev Vehicles STECH 93*, volume 2, pages 299–304, 1993.

[17] S. Ozawa, K. Murata, and T. Maeda. Effect of ballasted track on distortion of pressure wave in tunnel and emission of micro-pressure wave. In *Aerodynamics and Ventilation of Vehicle Tunnels, BHR Group, UK*, pages 935–947, 1997.

[18] S. Ozawa, T. Uchida, and T. Maeda. Reduction of micro-pressure wave radiated from tunnel exit by hood at tunnel entrance. *Quarterly reports of RTRI*, 19(2):77–83, 1978.

[19] M. Schultz and H. Sockel. The influence of unsteady friction on the propagation of pressure waves in tunnels. In *Aerodynamics and Ventilation of Vehicle Tunnels, Durham, UK*, pages 123–136. BHR Group, 1988.

[20] T. Tielkes, H.-J. Kaltenbach, M. Hieke, P. Deeg, and M. Eisenlauer. Measures to counteract micro-pressure waves radiating from tunnel exits of DB's new Nuremberg - Ingolstadt high - speed line. *Notes on Numerical Fluid Mechanics and Mulitdisciplinary Design. Vol. 99: Noise and Vibration Mitigation for Rail Transportation Systems, Proceedings of the 9th International Workshop on Railway Noise, Munich, 4 - 8 September 2007. Schulte-Werning, B. et al. (ed.).* Springer. 2008.

[21] Th. Tielkes. Aerodynamic Aspects of Maglev System. In R. Schach and M. Witt, editors, *MAGLEV'2006. The 19th International Conference on Magnetically Levitated Systems and Linear Drives. 13.-15. September 2006, Dresden, Germany. ISBN: 3-86005-535-6.*, pages 641–649, 2006.

[22] A.E. Vardy and J.M.B. Brown. Transient, turbulent, smooth pipe friction. *Journal of Hydraulic Research*, 33(4):435–456, 1995.

[23] A.E. Vardy and J.M.B. Brown. Influence of ballast on wave steepening in tunnels. *Journal of Sound and Vibration*, 238(4):595–615, 2000.

[24] A.E. Vardy and J.M.B. Brown. An overview of wave propagation in tunnels. *Notes on Numerical Fluid Mechanics: TRANSAERO - A European initiative on transient aerodynamics for railway system optimisation*, 79:249–266, 2002.

[25] A.E. Vardy and J.M.B. Brown. Transient turbulent friction in smooth pipe flows. *Journal of Sound and Vibration*, 259(5):1011–1036, 2003.

[26] A.E. Vardy and J.M.B. Brown. Efficient approximation of unsteady friction weighting functions. *Journal of Hydraulic Engineering*, 130(11):1097–1107, 2004.

[27] A.E. Vardy and J.M.B. Brown. Transient turbulent friction in fully rough pipe flows. *Journal of Sound and Vibration*, 270:233–257, 2004.

[28] A.E. Vardy, J.M.B. Brown, and H. Kuo-Lun. A weighting function model of transient turbulent pipe friction. *Journal of Hydraulic Research*, 31(4):533–548, 1993.

[29] W. Zielke. Frequency-dependent friction in transient pipe flow. *Journal of Basic Engineering*, 90(1):109–115, 1968.